



Multidimensional thermal mapping during radiofrequency ablation treatments with minimally invasive fiber optic sensors

GIOVANNA PALUMBO,¹ ELENA DE VITA,^{1,2} EMILIANO SCHENA,² CARLO MASSARONI,² PAOLO VERZE,³ NICOLA CARLOMAGNO,³ VINCENZO TAMMARO,³ ROBERTO LA ROCCA,³ JULIET IPPOLITO,³ DANIELE TOSI,^{4,5} PAOLA SACCOMANDI,⁶ MICHELE ARTURO CAPONERO,⁷ AGOSTINO IADICICCO,¹ AND STEFANIA CAMPOPIANO^{1,*}

¹Dept. of Engineering, University of Naples "Parthenope", Naples, Italy

²Università Campus Bio-Medico di Roma, Rome, Italy

³Dept. of Urology and Dept. of General Surgery University of Naples "Federico II" Naples, Italy

⁴Dept. of Electronic and Computer Engineering, Nazarbayev University, 010000 Astana, Kazakhstan

⁵National Laboratory Astana, Lab. of Biosensors and Bioinstruments, 010000 Astana, Kazakhstan

⁶Dept. of Mechanical Engineering, Politecnico di Milano, Italy

⁷Photonics Micro- and Nanostructures Laboratory, Research Center of Frascati-ENEA, Frascati, Rome, Italy

*stefania.campopiano@uniparthenope.it

Abstract: Temperature mapping is a key asset in supporting the clinician during thermal ablation (TA) treatment of tumors without adding additional risk to the TA procedure. Herein we report our experiments on multidimensional thermal mapping during radio frequency (RF) thermal ablation treatments of an *ex-vivo* animal organ. The temperature was monitored using several arrays of fiber Bragg gratings properly positioned around the RF applicator. The results show the effectiveness of our proposed method at assessing the TA probe depth and demonstrating how the insertion depth directly influences the maximum temperature and the treated area of the radio frequency ablation.

© 2018 Optical Society of America under the terms of the [OSA Open Access Publishing Agreement](#)

1. Introduction

Radiofrequency ablation (RFA) for removal of solid tumors is a minimally invasive thermo-ablative technique applied to the field of surgical oncology [1]. Its main advantage over more invasive procedures, particularly in surgical resectioning (such as the Pringle Manoeuvre in cases of hepatocellular carcinoma), is its minor impact on surgical stress thus allowing for faster recovery which is most important in old or very weak patients. RFA procedures can be applied percutaneously in both laparoscopic and open surgery, and are applicable to several types of tumors such as liver, kidney and lung, as well as in treating metastases such as hepatic metastases due to colorectal cancer [2–5]. RFA consists of electrodes inserted into a lesion which cause an electrical current flow. This phenomenon leads to frictional agitation at the ionic level and a consequent heat generation known as the Joule effect [1]. Thermal treatment brings about a localized increment of the organ's temperature with consequent tissue dehydration and water vaporization. In this way coagulation necrosis takes place; a term used to describe the irreversible thermal damage which biological tissues undergo. Indeed, RFA's aim is to destroy cancerous cells by exposing them to cytotoxic temperature while sparing the adjacent healthy tissue.

The mortality rate of tumor cells is a function of the temperature value reached within the organ and of the time exposure [6]. In this way real-time temperature monitoring, which

allows for adjustment of the RFA settings, can be considered valuable for achieving optimum clinical results. The knowledge of temperature during thermal ablation (TA) treatment gives the surgeon a way of controlling temperature distribution in the tissue surrounding the RF electrodes. This information reduces the need for repeated sessions to achieve complete necrosis for larger tumors [7] and the occurrence of potentially adverse effects to the surrounding healthy tissue [8]. Indeed, a deep insertion of the TA probe in the organ allows the heat to disperse to the blood vessels to better control eventual bleeding (a serious post-operative complication), but the risk of damaging the surrounding tissue increases. Therefore, the application time is eventually associated with an extended tissue damage which could be better controlled and limited when using an accurate temperature mapping.

RFA is generally carried out under ultrasound (US) guidance [9] which allows for precise positioning of the probe close to the target even during challenging procedures (e.g., intracavitary and endoluminal applications). However, accurate tumor localization alone is not sufficient for obtaining targeted treatment without damaging healthy surrounding tissue, as it does not allow quantifying cell's response to heat [10]. Indeed, it is still challenging to visualize the thermal dose delivered, and to delineate the damaged tissue margins with conventional US techniques because of the low intrinsic contrast between normal and ablated tissue and artefacts due to gas bubble formation [11]. It is for this reason that researchers have devised temperature maps by using a cross-correlation algorithm as applied to RF ultrasound echo signal data acquired at discrete intervals during heat treatment and caused by the speed of sound variation and thermal expansion with temperature. This thermometric technique however, requires calibration of the speed of sound variations and tissue expansion with temperature. Furthermore, US-based thermometry is affected by physiological motion and unexpected changes in acoustic properties of tissues [12]. Modern US systems are equipped with an image modality called Shear Waves Elastography (SWE), allowing to quantify tissue stiffness. Since a coagulated tissue is stiffer than a normal one, some studies are investigating the feasibility and accuracy of SWE for quantitative monitoring of thermal ablation [13]. Anyway, this technique is still in the early-stage, and cannot be expended to the monitoring of deep-seated lesions undergoing ablation therapy.

To overcome this limitation, several commercial RF probes are equipped with thermocouples in the tips of the electrodes which can measure the temperature of the adjacent tissue [12]. Nevertheless, this is not enough to accurately monitor temperature distribution of the tissue.

Other solutions aimed at visualizing three-dimensional temperature distribution in tissue during RFA procedures have been investigated such as the implementation of 3-D finite element models based on bio-heat equation whereby the results were corroborated with experimental data recovered through the use of thermocouples at the tip of the ablation electrodes [14]. However, the use of thermocouples may cause significant measurement errors due to their high thermal conductivity. Another solution to predict tissue destruction and cell death consists of a laparoscopic infrared camera capable of thermally mapping surface tissue temperatures [15]. The limitation of using a thermal camera however is that it is almost always limited to ex vivo analysis. Moreover, use of a laparoscopic thermal camera in clinical applications implies invasive surgical intervention and for this reason its level of invasiveness is incompatible with RFA which is a minimally invasive treatment [16].

The current landscape of temperature monitoring during RFA is facing with the challenges to obtain real-time and accurate temperature measurements by a minimally invasive approach. Therefore, multi-point temperature measurements performed with fiber Bragg grating sensors (FBGs) are a promising solution. FBG sensors have great potential in medicine, thanks to their biocompatibility, immunity to electromagnetic interference, non-toxicity, chemical inertness and small size [17]. Due to their unique features, several studies have been conducted on the use of these sensors for real-time temperature monitoring during RFA. Some studies focused on the monitoring of tissue temperature during RFA by means of

linearly chirped fiber Bragg gratings (LCFBGs) [16,18]. This promising solution for distributed sensing presents the drawback of no reliable technique for their detection in the spectrum domain. Indeed, certain spectrum decoding methods require an overwhelming complexity and are not affordable in real-time operation, while simplified approaches substantially turn the LCFBG into a few-point sensor, which does not offer relevant advantages over uniform FBGs.

The current technology allows writing multiple FBGs in a single fiber enabling multi-point temperature measurements with high spatial resolution, inserting only one fiber optic within organs. Accordingly, other studies investigated the potential of FBG array for monitoring temperature in this field. Tosi et al. had directly mounted the FBG array on the ablation device, providing 5 points real-time temperature measurements (1 sensor/cm).

Saccomandi et al. performed temperature measurements during CT-guided RFA performed with the StarBurst XL Electrosurgical Device. They used two custom-made thermal probes embedding a total of 9 FBGs (2 sensors/cm), in addition to the 5 thermocouples embedded in the umbrella-shaped RF probe. The multipoint temperature monitoring by using FBG sensors at several distances from the applicator provided useful and additional information regarding the boundary of damaged volume. The following table summarizes the principal details of some of the FBG-based temperature monitoring systems solutions proposed in the literature (see Table 1).

Table 1. Principal details of some of the fiber Bragg gratings-based temperature monitoring systems solutions proposed in the literature

Article	Type of sensor	RF probe	Model of ablation	Details of measuring approach
Tosi et al. 2014 [16,19,20]	LCFBG	Hollow brass needle with 3/4 mm inner/outer diameter and 10-mm length, for laparoscopic and percutaneous approaches	<i>Ex vivo</i> animal model (samples of porcine liver)	Real-time monitoring; 1 LCFBG for a quasi-distributed detection
Tosi et al. 2014 [19,21]	FBG	Hollow brass needle with 3/4 mm inner/outer diameter and 10-mm length, for laparoscopic and percutaneous approaches	<i>Ex vivo</i> animal model (samples of porcine liver)	Real-time monitoring; 1 FBG array; 5 measurement sites; spatial resolution of 1 sensor/cm
Samset et al. 2001 [22]	FBG	3 mm cryo probe (Galil Medical, Yokneam, Israel)	<i>In vivo</i> animal model (porcine liver)	2 FBG arrays; 20 measurement sites; spatial resolution of 2 sensors/cm
Saccomandi et al. 2016 [23]	FBG	MRI compatible StarBurst XL Electrosurgical Device, for laparoscopic and percutaneous approaches	<i>Ex vivo</i> animal model (porcine liver)	Real-time monitoring; 2 FBG arrays; 9 measurement sites; spatial resolution of 2 sensors/cm
Palumbo et al. 2016 [24]	FBG	Habib 4X, a laparoscopic bipolar RF device	<i>Ex vivo</i> animal model (liver and kidney)	Real-time monitoring; 5 measurement sites; spatial resolution of 5 mm

Building upon this research, we have recently proposed a FBG-equipped RFA probe for real-time monitoring of temperature during ablation, employing the Habib 4X RF commercial probe [25] measuring impedance between the electrodes as an indirect measure of temperature during ablation experiments. In previous reported experiments [24] researchers demonstrated that a linear FBG array was very useful for direct real-time temperature measure as it allows for potential optimization of the RF parameter (i.e. power and duration of the RF discharge).

Herein we present a significant improvement in the design of the sensorized RF probe based upon multidimensional temperature measurements. Its main strength is the housing of multiple FBG arrays with high spatial resolution, which provides increased valuable

information about the temperature of the RF treated area. This approach is clinically relevant since the surgeon usually evaluates and establishes the RF probe's insertion depth with the sole aim of reaching the cancerous tissue, disregarding the substantial temperature increase of the organ as the electrodes' depth increases.

Our previous studies analyzed the temperature map and the distance from the RF applicator axis along the treatment without focusing on the above-mentioned insertion depth [23,24]. Herein we show how the proposed system is able to measure the temperature profile around the RF probe assessing that the TA probe's insertion depth directly influences the maximum temperature and the treated area. The obtained temperature mapping is a key asset that can support the clinician during treatment, without added invasiveness and ensuing risk to the procedure. Our proposed setup and results obtained are detailed, described and commented upon below.

2. Experimental setup

FBGs consist of a segment of optical fiber along which a spatially periodic modulation of the core refractive index is permanently made. The index modulation leads to the reflection of light in a narrow range of wavelengths while other wavelengths are transmitted along the fiber. The reflected range of wavelengths are centered on a specific value known as the Bragg wavelength λ_B , which is expressed as: $\lambda_B = 2n_{\text{eff}}\Lambda$, where n_{eff} is the effective refractive index of the guided core mode and Λ is the grating period. The grating is intrinsically a strain and temperature sensor and the external physical parameters are detected through the measurement of the reflected wavelength. For our purposes, the FBGs were employed in a strain-free configuration in order to consider the temperature contribution only, which is linearly related to the Bragg wavelength shift with the following expression: $\Delta\lambda_B/\lambda_B = S_T\Delta T$, where S_T is the thermal sensitivity coefficient of the grating [26].

In our experiments the Habib 4x laparoscopic bipolar Device RF probe was employed and consisted of 10 cm long electrodes (6 cm of inactive part and 4 cm of active part) that allowed for RF current circulation in a pig liver) [27]. Figure 1 shows the RF probe outfitted with 5 arrays for a total 27 FBGs representing the measurement sites. This configuration allowed for the processing of two-dimensional thermal maps in planes perpendicular and parallel to the probe's electrodes with a resolution of 0.1 °C.

FBG commercial arrays with the following characteristics were used in conducting the tests:

- Array A of 3 FBGs - length of each grating 1 mm and distance edge-to-edge 3 mm. Total length of 9 mm at $x = -0.70$ cm;
- Array B of 7 FBGs - length of each grating 1 mm and distance edge-to-edge 2 mm. Total length of 19 mm at $x = 0.35$ cm;
- Array C of 10 FBGs - length of each grating 1 mm and distance edge-to-edge 2 mm. Total length of 28 mm at $x = 0.00$ cm;
- Array D of 3 FBGs - length of each grating 1 mm and distance edge-to-edge 3 mm. Total length of 9 mm at $x = 0.70$ cm;
- Array E of 4 FBGs - length of each grating 1 mm and distance edge-to-edge 3 mm. Total length of 13 mm at $x = 1.05$ cm.

Four FBG arrays were positioned at $x = 0.00$ cm, $x = 0.35$ cm, $x = 0.70$ cm and $x = 1.05$ cm in order to measure a temperature profile starting from the electrode's center. The last array was fixed at $x = -0.70$ cm to observe the symmetry of the temperature profile. Due to the length of the electrodes, a plexiglass support for the FBGs sensors was also fabricated to facilitate their positioning and make the structure easily removable from the RF probe, Fig. 1(b). The FBG sensors were then inserted into carbon fiber microtubes with an inner diameter

of 0.30 mm and an outer diameter of 0.70 mm. The microtubes were securely fixed to the plexiglass support and positioned about 1 cm deeper than the electrodes' tip to monitor a larger area. Finally, the ends of the microtubes were accurately pointed to easily insert the RF probe into the organ and avoid a possible bending of the needles, Fig. 1(c).

Several test have been carried out, by inserting and extracting the probe into the animal tissues, in order to verify that the carbon fiber microtubes do not transmit the strain to the FBGs inserted into them.

Furthermore, in Fig. 1(d), the optical reflected spectrum of the array C is shown.

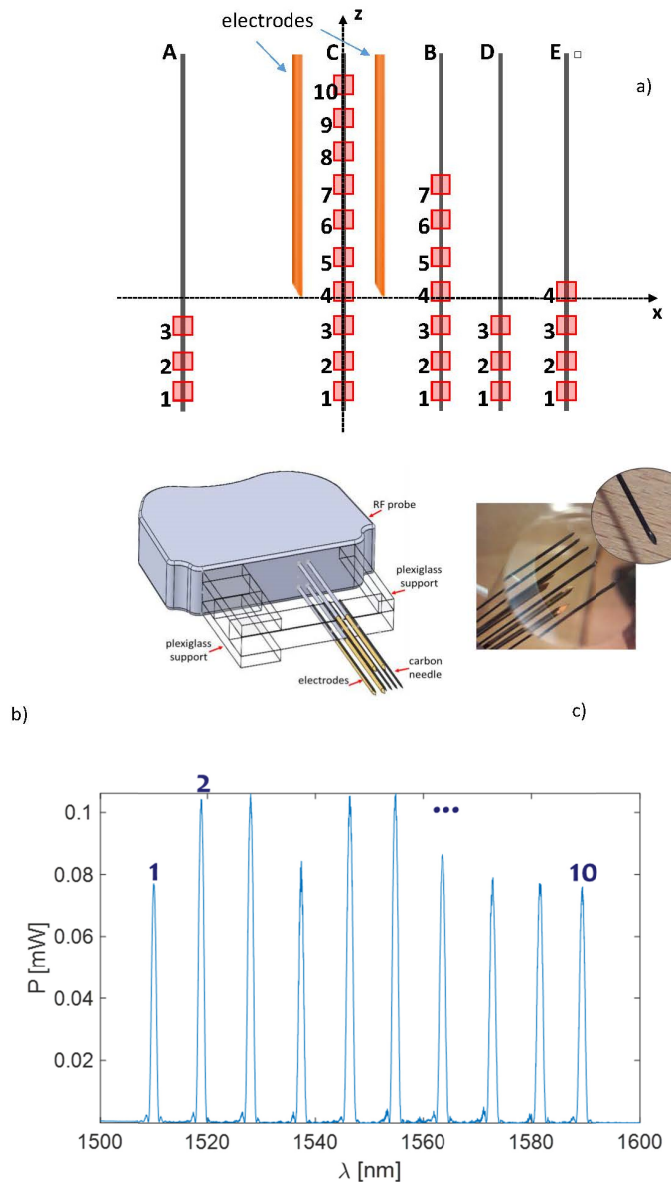


Fig. 1. a) Schematic of the array of FBGs embedded within the probe; b) Schematic of modified RF probe; c) Detail of carbon needle; c) FBG sensors arrangement; d) Array C optical reflected spectrum.

Figure 2 presents a picture of the experimental setup, including: 1) the RF device powered by a 500 kHz generator (Model 1500X Rita Medical Systems, Inc. California, USA) with a maximum power of 250 W [28]; 2) the optical interrogation system (Model FS-22 HBM BraggMETER) which includes a tunable laser operating in the range of 1500 to 1600 nm and is equipped with eight optical channels allowing for simultaneous measurement of a large number of sensors (up to 25 for each channel). The detector measures the Bragg wavelengths with a resolution of 1 pm making possible to detect temperature with a resolution of 0.1 °C, with a minimum sampling frequency of 1 Hz [29,30]; 3) the PC; 4) the modified RF probe; 5) a thermocouple used as a reference.



Fig. 2. Experimental setup.

3. Results and discussions

Experiments were carried on *ex vivo* pig liver tissue at the Urology Dept. of the University of Naples Federico II “Policlinico” Hospital. Tests included varying the insertion depth of the RF probe and maintaining the same parameters of the RF discharge. The main objective was to compare the effect of discharges at different tissue depths. The FBG sensors had been previously thermally characterized resulting in thermal sensitivity coefficients (S_T) between $6.4 \cdot 10^{-6}$ and $6.7 \cdot 10^{-6} \text{ } ^\circ\text{C}^{-1}$.

3.1 Experiments on *ex vivo* animal liver

Figure 3 shows the results of two RF discharges on the *ex vivo* animal liver. The temperatures recorded by the FBGs positioned at the same height as the discharged electrodes are shown. The temperature data versus spatial position were achieved by a piecewise linear interpolation of the experimental data points. In Fig. 3, temperature is reported by a color map versus spatial sensor position (vertical axis in the graph) and time (horizontal axis). Positions of the used arrays are shown to the left of Fig. 3. The two RF discharges at an insertion depth of 2.5 cm and 4.0 cm, respectively can be easily distinguished. The first discharge reached temperatures not higher than 100 °C and the recorded temperature values are in accordance with the sensors' position: the highest temperature is recorded by the sensors near the electrodes and a temperature around 80 °C is recorded by the sensors positioned beyond 0.5 cm from the electrodes. During the second discharge performed on another organ region, a temperature above 120 °C was recorded; the maximum peak was experienced by the FBG of

array A positioned at -0.70 cm, probably due to the proximity of the needle to the application area of the RFA.

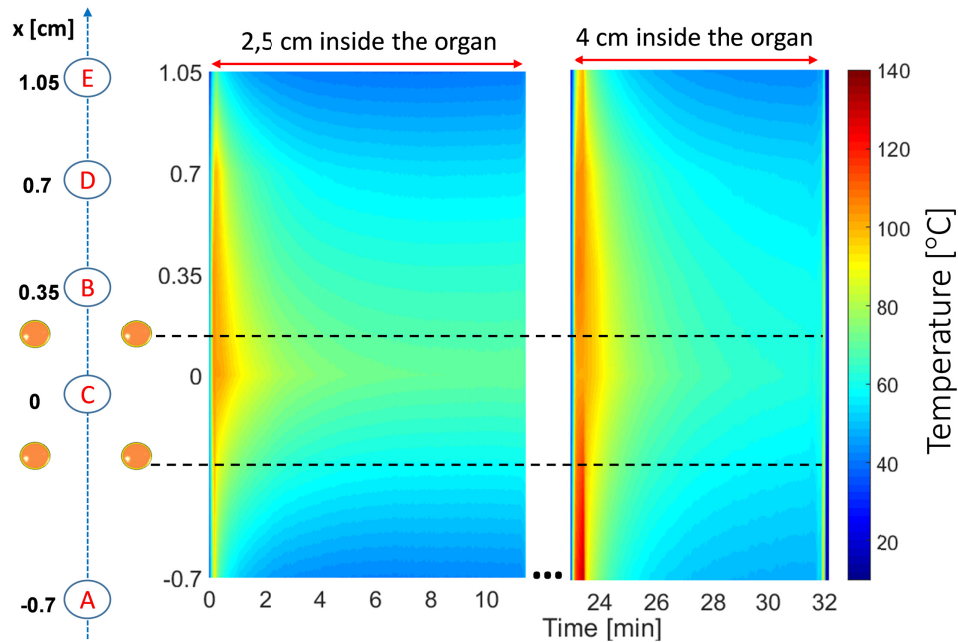


Fig. 3. Temperature profile of the FBGs at the end of the tip of the electrodes.

Figure 4 shows the temperature space-time map of array C positioned at the center of the discharge electrodes during two discharges at the same depth as in the previous test. As in previous tests, temperature data versus spatial position were achieved by a piecewise linear interpolation of the experimental data points. For clarity, we numbered the 10 FBGs of the array starting from the bottom so that the fourth sensor of the array was located at the same height as the tips of the electrodes (indicated with the dashed black line). The temperature recorded during the first discharge was quite uniform for the 10 FBGs of the array, indeed it went from a maximum ΔT of 85.5 °C read by sensor 4 to a minimum of 80.3 °C recorded by FBG 1 on the tip of the array, i.e. the sensor which was placed deeper than the probe electrodes. This behavior is reasonable because the sensors placed deeper than the actual tip of the electrodes will read a slightly lower temperature with respect to the sensors positioned near the tip of the electrodes.

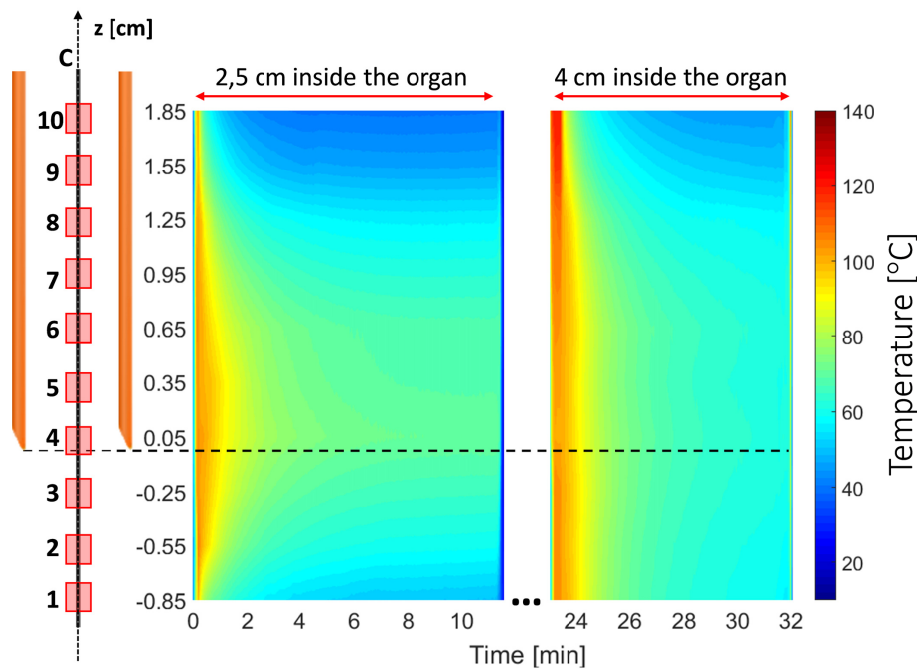


Fig. 4. Temperature profile of the 10 FBG sensors of the array C.

After the first discharge the RF probe was extracted from the liver sample and returned to room temperature. After about 10 minutes it was reinserted at another point and a second RF discharge was applied. For the second discharge a temperature of about 100 °C was recorded by FBG 9 and FBG 10, located at a distance of 1.55 and 1.85 cm from the electrodes' tip, respectively. For the other sensors, the ΔT ranged between 88 °C and 85 °C.

Figure 5 reports four tests carried out at four different depths on the *ex vivo* animal liver sample. The temperature variation with respect to the z axis, i.e. the vertical position of the arrays on the RF probe is shown. When the insertion depth increases, the temperature increases accordingly: a ΔT of 50.1 °C was registered for a depth of 0.5 cm, whereas a ΔT of 97.1 °C registered at an insertion depth of 3.5 cm.

Figure 5(a), shows that array B (positioned at $x = 0.35$ cm) recorded the maximum temperature at a depth of 0.5 cm, while the temperature profile shown by array C (blue line) experienced a lower temperature but was extended along the whole array (about 28 mm). Arrays A and D underwent comparable temperature increases while, as expected, the temperature increment recorded by array E (positioned at $x = 1.05$ cm) was negligible. A similar behavior occurs at a depth of 1.5 cm and 2.5 cm as shown in Fig. 5(b)-(c), respectively. However in these cases the maximum temperature was recorded by the array positioned at the center of the probe with an increasingly distributed temperature profile along the entire dimension of the array. It can also be noted that, at a distance of about 1 cm from the center of the electrodes, the temperature tended to gradually decrease and that for greater depths a temperature variation was recorded at distances even further than 1 cm (array E with $\Delta T \neq 0$).

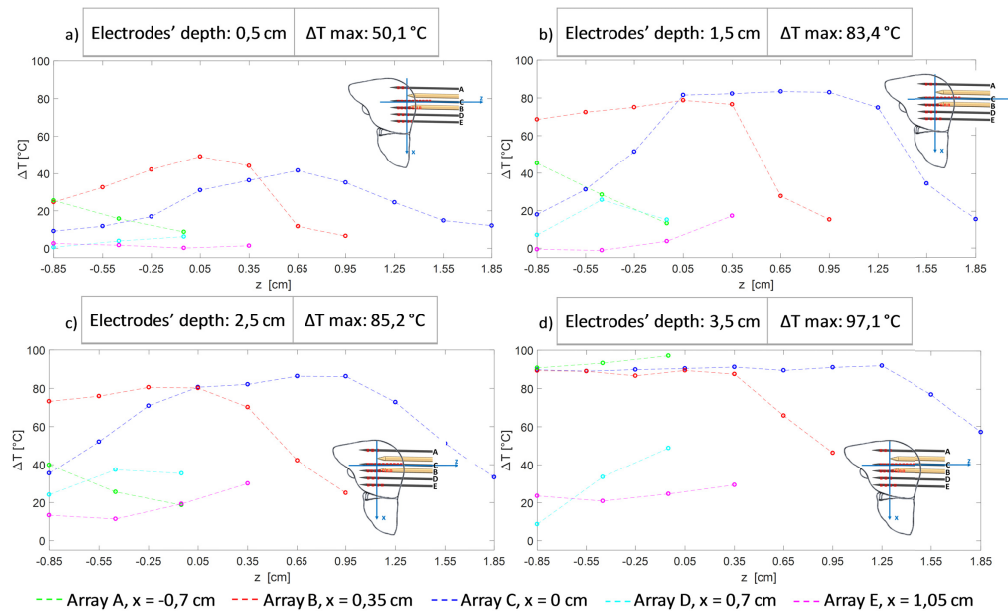


Fig. 5. Temperature variation at different depths of the RF probe insertion in liver sample.

Finally, Fig. 5(d) shows the test for a discharge made at 3.5 cm depth. In this test the maximum temperature was recorded by array A, most likely because the carbon needle had moved slightly closer to the center of the electrodes. The trends of arrays B and C are in accordance with what had already been observed, i.e. array C recorded a higher and more evenly distributed temperature. The ΔT recorded by arrays D and E was higher than in previous tests: the maximum temperature for arrays D and E respectively are registered are $\Delta T_{\max} = 48.8$ °C and $\Delta T_{\max} = 29.3$ °C. The effects of the RF discharges at different depths are also reported in Fig. 6. When the insertion depth increases, the maximum temperature recorded increases as well and the necrotized zone increases accordingly. This effect is due to the necessity to necrotize an increasingly larger area so that the RF device will have to emit a longer RF pulse (at a fixed RF power), resulting in an increase in temperature and in the width of the damaged area. Furthermore, the deeper is the insertion the more vascularized is the interested area with a consequent thermal improvement. Therefore, the effects of the discharge lead to a greater lesion both in terms of the height and width of the damage.

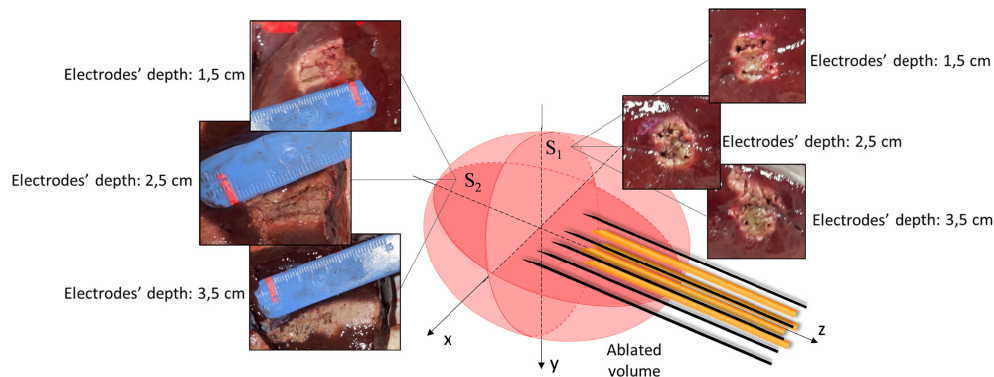


Fig. 6. Effects of discharges at different depths of RF probe insertion.

Figure 7 presents a detail of the test discussed in Fig. 5, i.e. the temperature variation recorded by array C during the four discharges at different depths. As can be seen from the figure, as the insertion depth increases, the maximum temperature peak increases as well and the temperature profile becomes more homogeneously distributed along the entire dimension of the array (from -0.85 cm to 1.85 cm).

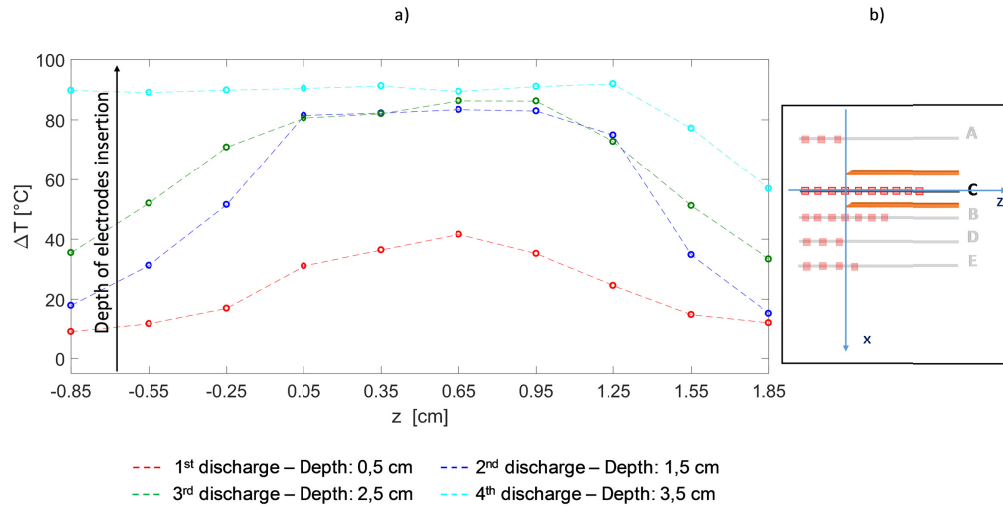


Fig. 7. a) Temperature variation of array C ($x = 0$) at different depths of the RF probe insertion in liver sample; b) Schematic of array C position with respect to the other arrays.

In particular, for a depth of 0.5 cm a $\Delta T_{\max} = 41.6$ °C at 0.65 cm (FBG 6) was measured, while for a depth of 1.5 cm a ΔT of circa 82.5 °C was recorded for a region length of about 1.20 cm (from 0.05 cm position of the FBG 4 sensor to 1.25 cm). A similar situation was observed for a discharge at a 2.5 cm depth, where a ΔT higher than 77 °C was recorded at a distance of 0.05 cm (tip of the electrodes) up to a distance of 0.95 cm (FBG 7). Finally, in the fourth discharge the temperature had a value higher than 89 °C and remained value up to a distance of 1.55 cm. Figure 7(b) reports the schematic of the position of array C.

4. Conclusion

Herein we propose a real-time multidimensional system for the thermal monitoring of RF treatments. While the aim of our previous experiments was the estimation of axial temperature distribution (i.e., along the direction of the ablation device or along its perpendicular by using multiple standard FBGs), herein we show that, using more FBG arrays gives a complete spatial temperature profile leading to important RF thermal treatment knowledge.

The evidence emerging from our experiments has important clinical implications because it clearly demonstrates how the effects of RFA can be influenced by several factors. We have assessed that the depth at which energy is applied influences the thermal effect on the tissue. The clinical relapse of such a process is easily understandable and of great importance and further emphasizes the necessity of ultra-precise measurements of the thermal gradient determined in the parenchyma and in the area surrounding the radiofrequency application site. The main limitation of our study is that the RFA was performed in *ex vivo* animal model. So the reliability of the results in a clinical context remains to be clarified. Indeed several factors may affect the results, such as the physiological perfusion status and baseline temperature of the organ. In consideration of this, it is expected that further phases in clinical trials will be developed to confirm the evidence currently available that has emerged from our study.

Funding

D. Tosi acknowledges the support of ORAU program at Nazarbayev University (grant LIFESTART). G. Palumbo, A. Iadicicco and S. Campopiano acknowledge the support of the “Bando di sostegno alla ricerca individuale per triennio 2015-2017, Annualità 2017” by the University of Naples “Parthenope”.

Acknowledgments

Nazarbayev University (grant LIFESTART); University of Naples “Parthenope”.

Disclosures

The authors declare that there are no conflicts of interest related to this article.

References

1. M. Ahmed, C. L. Brace, F. T. Lee, Jr., and S. N. Goldberg, “Principles of and Advances in Percutaneous Ablation,” *Radiology* **258**(2), 351–369 (2011).
2. L. M. Sutherland, J. A. R. Williams, R. T. A. Padbury, D. C. Gotley, B. Stokes, and G. J. Maddern, “Radiofrequency Ablation of Liver Tumors: A Systematic review,” *Arch. Surg.* **141**(2), 181–190 (2006).
3. D. A. Kunkle and R. G. Uzzo, “Cryoablation or radiofrequency ablation of the small renal mass : a meta-analysis,” *Cancer* **113**(10), 2671–2680 (2008).
4. T. de Baère, J. Palussière, A. Aupérin, A. Hakime, M. Abdel-Rehim, M. Kind, C. Dromain, A. Ravaud, N. Tebboune, V. Boige, D. Malka, C. Lafont, and M. Ducreux, “Midterm Local Efficacy and Survival after Radiofrequency Ablation of Lung Tumors with Minimum Follow-up of 1 Year: Prospective Evaluation,” *Radiology* **240**(2), 587–596 (2006).
5. S. L. Wong, P. B. Mangu, M. A. Choti, T. S. Crocenzi, G. D. Dodd 3rd, G. S. Dorfman, C. Eng, Y. Fong, A. F. Giusti, D. Lu, T. A. Marsland, R. Michelson, G. J. Poston, D. Schrag, J. Seidenfeld, and A. B. Benson 3rd, “American Society of Clinical Oncology 2009 clinical evidence review on radiofrequency ablation of hepatic metastases from colorectal cancer,” *J. Clin. Oncol.* **28**(3), 493–508 (2010).
6. D. Haemmerich, “Biophysics of Radiofrequency Ablation,” *Crit. Rev. Biomed. Eng.* **38**(1), 53–63 (2010).
7. R. I. Carey and R. J. Leveillee, “First Prize: Direct Real-Time Temperature Monitoring for Laparoscopic and CT-Guided Radiofrequency Ablation of Renal Tumors between 3 and 5 cm,” *J. Endourol.* **21**(8), 807–813 (2007).
8. P. Saccomandi, E. Schena, and S. Silvestri, “Techniques for temperature monitoring during laser-induced thermotherapy: an overview,” *Int. J. Hyperthermia* **29**(7), 609–619 (2013).
9. S. N. Goldberg, G. S. Gazelle, and P. R. Mueller, “Thermal Ablation Therapy for Focal Malignancy: A Unified Approach to Underlying Principles, Techniques, and Diagnostic Imaging Guidance,” *AJR Am. J. Roentgenol.* **174**(2), 323–331 (2000).
10. E. Schena, D. Tosi, P. Saccomandi, E. Lewis, and T. Kim, “Fiber Optic Sensors for Temperature Monitoring during Thermal Treatments: An Overview,” *Sensors (Basel)* **16**(7), 1144 (2016).
11. T. Varghese, J. A. Zagzebski, Q. Chen, U. Techavipoo, G. Frank, C. Johnson, A. Wright, and F. T. Lee, Jr., “Ultrasound monitoring of temperature change during radiofrequency ablation: preliminary in-vivo results,” *Ultrasound Med. Biol.* **28**(3), 321–329 (2002).
12. J. P. McGhana and G. D. Dodd 3rd, “Radiofrequency Ablation of the Liver: Current Status,” *AJR Am. J. Roentgenol.* **176**(1), 3–16 (2001).
13. E. S. Broesses, M. Pernot, and M. Tanter, “The link between tissue elasticity and thermal dose in vivo,” *Phys. Med. Biol.* **56**(24), 7755–7765 (2011).
14. D. Panescu, J. G. Wayne, S. D. Fleischman, M. S. Mirotznik, D. K. Swanson, and J. G. Webster, “Three-dimensional finite element analysis of current density and temperature distributions during radio-frequency ablation,” *IEEE Trans. Biomed. Eng.* **42**(9), 879–890 (1995).
15. K. Ogan, W. W. Roberts, D. M. Wilhelm, L. Bonnell, D. Leiner, G. Lindberg, L. R. Kavoussi, and J. A. Cadeddu, “Infrared thermography and thermocouple mapping of radiofrequency renal ablation to assess treatment adequacy and ablation margins,” *Urology* **62**(1), 146–151 (2003).
16. D. Tosi, E. G. Macchi, M. Gallati, G. Braschi, A. Cigada, S. Rossi, G. Leen, and E. Lewis, “Fiber-optic chirped FBG for distributed thermal monitoring of ex-vivo radiofrequency ablation of liver,” *Biomed. Opt. Express* **5**(6), 1799–1811 (2014).
17. S. Silvestri and E. Schena, “Optical-Fiber Measurement Systems for Medical Applications,” in *Optoelectronics* (Intech, 2011), p. 642.
18. G. Palumbo, D. Tosi, A. Iadicicco, and S. Campopiano, “Analysis and design of chirped fiber Bragg grating for temperature sensing in biomedical applications,” *IEEE Sensors*, under review (2018).
19. D. Tosi, E. G. Macchi, and A. Cigada, “Fiber-optic temperature and pressure sensors applied to radiofrequency thermal ablation in liver phantom: Methodology and experimental measurements,” *J. Sens.* **2015**, 1 (2015).

20. E. G. Macchi, D. Tosi, G. Braschi, M. Gallati, A. Cigada, G. Busca, and E. Lewis, "Optical fiber sensors-based temperature distribution measurement in ex vivo radiofrequency ablation with submillimeter resolution," *J. Biomed. Opt.* **19**(11), 117004 (2014).
21. D. Tosi, E. Macchi, G. Braschi, and M. Gallati, "Monitoring of radiofrequency thermal ablation in liver tissue through fibre Bragg grating sensors array," *Electron. Lett.* **50**(14), 981–983 (2014).
22. E. Samset, T. Mala, R. Ellingsen, I. Gladhaug, O. Søreide, and E. Fosse, "Temperature measurement in soft tissue using a distributed fibre Bragg-grating sensor system," *Minim. Invasive Ther. Allied Technol.* **10**(2), 89–93 (2001).
23. P. Saccomandi, E. Schena, M. Diana, F. M. Di Matteo, G. Costamagna, and J. Marescaux, "Multipoint temperature monitoring in liver undergoing computed tomography-guided radiofrequency ablation with fiber Bragg grating probes," in *2016 38th Annual International Conference of the IEEE Engineering in Medicine and Biology Society (EMBC)* (IEEE, 2016), pp. 5174–5179.
24. G. Palumbo, A. Iadicicco, D. Tosi, P. Verze, N. Carlomagno, V. Tammaro, J. Ippolito, and S. Campopiano, "Temperature profile of ex-vivo organs during radio frequency thermal ablation by fiber Bragg gratings," *J. Biomed. Opt.* **21**(11), 117003 (2016).
25. L. R. Jiao, P. D. Hansen, R. Havlik, R. R. Mitry, M. Pignatelli, and N. Habib, "Clinical short-term results of radiofrequency ablation in primary and secondary liver tumors," *Am. J. Surg.* **177**(4), 303–306 (1999).
26. Q. Yu, Y. Zhang, Y. Dong, Y. P. Li, C. Wang, and H. Chen, "Study on Optical Fiber Bragg Grating Temperature Sensors for Human Body Temperature Monitoring," in *2012 IEEE Symposium on Photonics and Optoelectronics* (IEEE, 2012).
27. Angiodynamics, "Habib 4x Bipolar Resection Device," <http://www.angiodynamics.com/products/habib-4x>.
28. "User's Guide and Service Manual RITA 1500X," AngioDynamics Inc. (n.d.).
29. HBM, "FS22 BraggMeter industriale," <https://www.hbm.com/it/4604/fs22-interrogatore-ottico-braggmeter-industriale/>.
30. HBM, FS22 User Manual (n.d.).